RESEARCH ARTICLE | OCTOBER 24 2023

Demonstration of near-ideal Schottky contacts to Si-doped AIN ⊕⊘

C. E. Quiñones \square \square ; D. Khachariya \square ; P. Bagheri \square ; P. Reddy \square ; S. Mita; R. Kirste \square ; S. Rathkanthiwar \square ; J. Tweedie; S. Pavlidis \square ; E. Kohn; R. Collazo \square ; Z. Sitar \square



Appl. Phys. Lett. 123, 172103 (2023) https://doi.org/10.1063/5.0174524





CrossMark





Cite as: Appl. Phys. Lett. **123**, 172103 (2023); doi: 10.1063/5.0174524 Submitted: 31 August 2023 · Accepted: 5 October 2023 · Published Online: 24 October 2023







C. E. Quiñones,^{1,a)} (b) D. Khachariya,² (b) P. Bagheri,¹ (b) P. Reddy,² (b) S. Mita,² R. Kirste,² (b) S. Rathkanthiwar,¹ (b) J. Tweedie,² S. Pavlidis,³ (b) E. Kohn,¹ R. Collazo,¹ (b) and Z. Sitar^{1,2} (b)

AFFILIATIONS

ABSTRACT

Near-ideal behavior in Schottky contacts to Si-doped AlN was observed as evidenced by a low ideality factor of 1.5 at room temperature. A temperature-independent Schottky barrier height of $1.9\,\mathrm{eV}$ was extracted from temperature-dependent I–V measurements. An activation energy of $\sim 300\,\mathrm{meV}$ was observed in the series resistance, which corresponded to the ionization energy of the deep Si donor state. Both Ohmic and Schottky contacts were stable up to $650\,^{\circ}\mathrm{C}$, with around four orders of magnitude rectification at this elevated temperature. These results demonstrate the potential of AlN as a platform for power devices capable of operating in extreme environments.

Published under an exclusive license by AIP Publishing. https://doi.org/10.1063/5.0174524

Aluminum nitride (AlN) is an attractive material for kV-class power electronics due to its extreme bandgap, high thermal conductivity (375 W/mK), and high critical field (16 MV/cm). 1-5 These properties result in a Baliga's figure of merit that is more than 30-times larger than that of other materials used in power applications, such as GaN and SiC. Moreover, AlN has a very high thermal and chemical stability, which makes it an ideal material system for applications under extreme environments. However, the development of AlN devices has been limited. Particularly, Schottky diodes fabricated on AlN show poor performance, with typical devices having ideality factor >5, high leakage current, and high ON-resistance.6-10 Furthermore, the barrier height for Schottky contacts to AlN is expected to be >2 eV, independent of the metal used. 11-13 However, this value has not been observed in Schottky diodes reported in the literature, with typical reported values ranging from 0.9 to 1.1 eV.6-10 Additionally, all reported Schottky barrier heights are temperature dependent, indicating contact inhomogeneity.

The observed poor device performance can be attributed to (1) the use of foreign substrates and (2) the lack of controllable doping. Foreign substrates like sapphire or SiC introduce copious dislocations and defects, which act as parallel leakage paths and compensators, and degrade device performance. Moreover, the lack of controllable doping has made the formation of high-quality Schottky and Ohmic contacts difficult. In recent years, there have been significant advances that

directly address these challenges. Specifically, the commercialization of bulk AlN single crystal substrates^{1,2,14–17} has enabled high-quality homoepitaxial AlN thin-film growth, ^{18,19} with average dislocation densities on the order of 10³ cm⁻². Additionally, the development of point defect management methods, ^{20–22} along with the achievement of controllable n-type doping in AlN, ^{23–26} has addressed the doping problem directly, paving the way for realizing practical devices on AlN. Based on these advances, we report near-ideal behavior in Schottky contacts to homoepitaxial Si-doped AlN. The contacts show a temperature-independent Schottky barrier height of 1.9 eV, a record low ideality factor of 1.5, low reverse leakage current, and a high-temperature stability up to 650 °C under high-vacuum conditions.

AlN films were grown on a c-oriented, single crystal AlN wafer in a vertical, low-pressure (20 Torr), inductively (RF) heated, metalorganic chemical vapor deposition (MOCVD) reactor. The AlN substrate was obtained from HexaTech and had an average dislocation density of $10^3 \, \rm cm^{-2}$. Before epitaxial growth, the substrate was first cleaned in organic solvents (acetone, IPA), followed by an acid clean (HCl, HF). Finally, the substrates were loaded into the reactor and annealed under NH₃ at 1100 °C. More details on substrate preparation can be found in other publications. 18,19,27 Trimethylaluminum (TMA), silane (SiH₄), and ammonia (NH₃) were used as the aluminum, silicon, and nitrogen precursors, respectively. A 1 μ m thick, unintentionally doped (UID), insulating AlN layer was grown on the AlN substrate at

¹Department of Materials Science and Engineering, North Carolina State University, Raleigh, North Carolina 27606, USA

²Adroit Materials, Cary, North Carolina 27518, USA

³Department of Electrical and Computer Engineering, North Carolina State University, Raleigh, North Carolina 27606, USA

^{a)}Author to whom correspondence should be addressed: cequinon@ncsu.edu

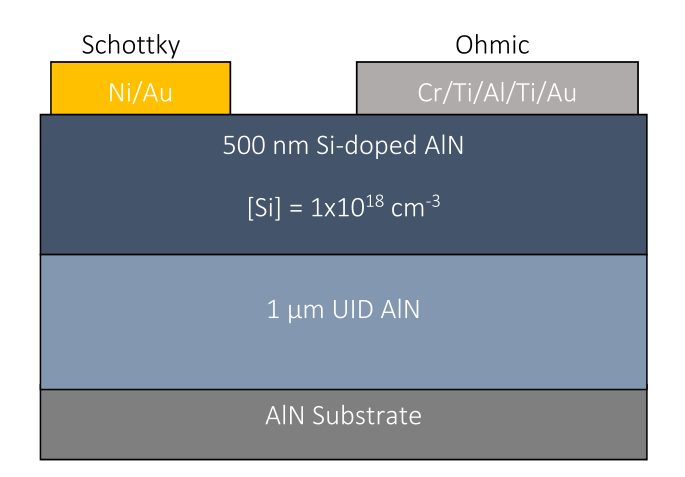


FIG. 1. Schematic cross section of the prepared AIN device test structure.

a temperature of 1300 °C, pressure of 20 Torr, NH₃ flow rate of 3 slm, and a V/III ratio of 6000 (TMA flow of 22 µmol/min). This was followed by 500 nm of Si-doped AlN, grown under the same pressure, temperature, and precursor flows. For the Si-doped layer, a SiH₄ flow of 7 nmol/min was used for a target Si concentration of $1 \times 10^{18} \text{ cm}^{-3}$. The grown AlN layers had a dislocation density of $\sim 10^3$ estimated by x-ray diffraction and an RMS roughness of <1 nm as measured by atomic force microscopy.²³ The sample structure is schematically shown in Fig. 1. The room temperature carrier concentration, mobility, and resistivity were found by AC Hall measurements to be 1.5×10^{15} cm⁻³, 160 cm²/V s, and 26 Ω -cm, respectively.²³ These measurements were performed using an 8400 series Lakeshore AC/DC Hall measurement system with contacts in the van der Pauw configuration. The temperature dependent Hall measurements for this particular sample have been previously published in Ref. 23. A more detailed analysis of the electrical properties and Hall measurements can be found there. It should be noted here that Si is in the deep donor state;²⁸ the carrier concentration is on the order of $10^{15} \, \mathrm{cm}^{-3}$ for a [Si] of $\sim 10^{18} \, \mathrm{cm}^{-3}$. Ohmic contacts were formed with a Cr/Ti/Al/Ti/Au (20/20/100/45/55 nm) metal stack, annealed at 950 °C for 30 s under nitrogen ambient. Schottky contacts consisted of circular Ni/Au (70/70 nm) metal

stacks, ranging from 70 to $600\,\mu\mathrm{m}$ in diameter, while the Ohmic contact was a large area rectangle (on the order of a few mm²). All contacts were defined using a shadow mask, rather than lithography, which led to a lateral Schottky-Ohmic contact spacing ranging from hundreds of $\mu\mathrm{m}$ to a few mm. Current– voltage (I–V) as well as impedance spectroscopy measurements were performed using a Keithley 4200 semiconductor characterization system. I–V measurements were done on $70\,\mu\mathrm{m}$ diameter diodes, whereas impedance measurements were performed on $600\,\mu\mathrm{m}$ diameter diodes. All measurements at elevated temperatures were performed under high-vacuum conditions.

The room temperature I-V characteristics for multiple Schottky contacts to AlN are shown in Fig. 2. In the reverse bias, less than 1 nA was observed at $-200\,\mathrm{V}$. In the forward bias, an exponential current region was observed close to 2 V. In this region, the ideality factor ranged from 1.5 to 1.7, as shown in Fig. 2(a). This is evidence that the current was mainly due to thermionic emission, as expected for ideal Schottky diodes. However, for biases much less than the barrier height, the electron current due to thermionic emission is very low, as electrons do not have enough energy to overcome the Schottky barrier. Since the thermionic emission current is so low, leakage current through parasitic pathways (i.e., dislocations and defects) dominates the I-V in this region. As the bias is increased and the barrier height is lowered, thermionic emission current grows and eventually becomes greater than the leakage current; this happened at around 2 V forward bias for all diodes. On the other hand, for forward bias voltages larger than 20 V, the I-V became linear, indicating that the current was limited by a series resistance, as shown in Fig. 2(c).

Although the bandgap of AlN is 6.1 eV, the current limitation arising from the series resistance of the Si-doped layer becomes apparent only after $\sim\!20\,\mathrm{V}$ of forward bias. This identification is supported the impedance spectrum of the device. The Nyquist plot for the contacts is shown in Fig. 3(a) for frequencies from 5 kHz to 10 MHz. Clearly, the single parallel RC equivalent circuit that is commonly used to model Schottky contacts is not sufficient to explain the observed frequency response. In fact, the contribution from three distinct parallel RC elements was observed, as shown by solid lines in Fig. 3(a). Therefore, to extract the three distinct contributions to the impedance, an equivalent circuit model with three parallel RC elements connected in series was used. Analytically, the complex impedance of the RC network is found to be

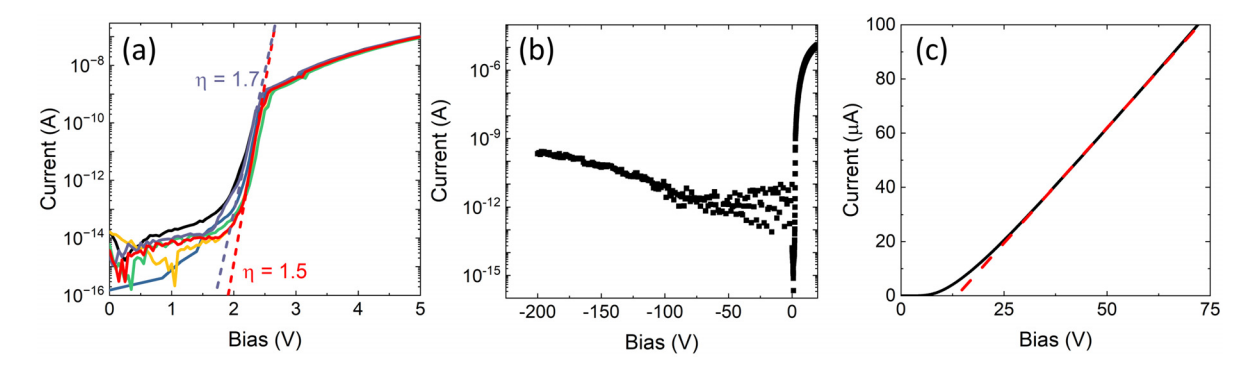


FIG. 2. (a) Room temperature forward bias I–V in the semi-log scale showing the low ideality factor for six distinct Schottky contacts. (b) Room temperature reverse bias I–V in the semi-log scale. (c) Room temperature forward bias I–V in the linear scale, showing the series resistance after ~20 V.

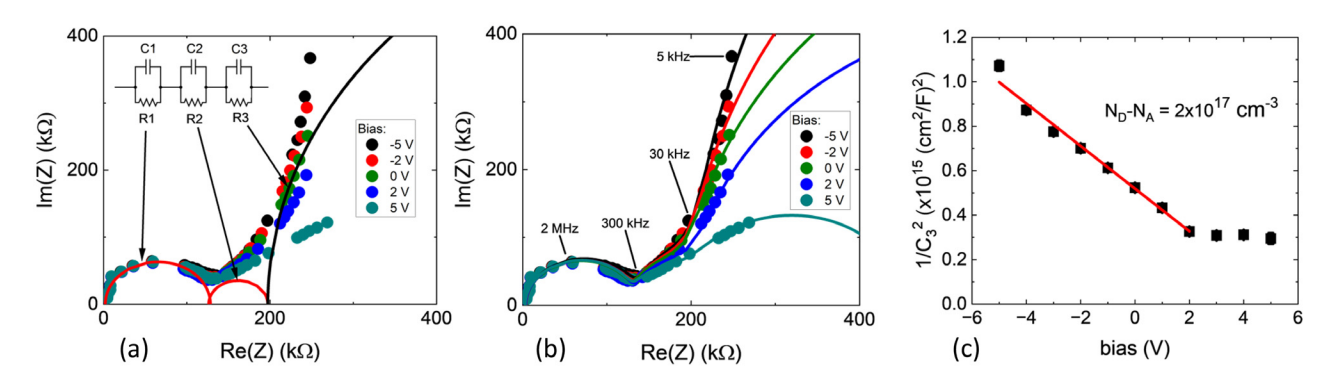


FIG. 3. (a) Room temperature Nyquist plot for bias from -5 to +5 V. The solid lines show the individual contribution the three parallel RC elements to the total impedance. The red semicircles indicate the bias-independent RC elements found from the impedance analysis. (b) Nyquist plot showing the results of curve fitting. Symbols are measured data; solid lines are the line fits to the triple RC equivalent circuit model. (c) $1/C^2$ vs bias plot for the bias dependent capacitance extracted using the presented model. A line fit yields $N_D - N_A = 2 \times 10^{17}$ cm⁻³.

$$Z = \sum_{i=1}^{3} \frac{1}{R_i^{-1} + j\omega C_i}.$$

Here, R_i are the resistances and C_i are the capacitances of the individual RC elements. From this, the real part of the impedance as a function of frequency is found as

$$Re(Z) = \sum_{i=1}^{3} \frac{1}{R_i(R_i^{-2} + \omega^2 C_i^2)} = |Z|\cos\theta$$

and the imaginary part as

$$Im(Z) = \sum_{i=1}^{3} \frac{-\omega C_i}{\left(R_i^{-2} + \omega^2 C_i^2\right)} = |Z| sin \ \theta. \label{eq:energy}$$

These equations are fitted to the experimental Im(Z) and Re(Z) as a function of frequency, and the values of the circuit elements are found as fitting parameters for a given bias. The fitted curves are shown in Fig. 3(b) as solid lines for biases ranging from -5 to +5 V. This analysis reveals a bias-dependent RC element at low frequencies (R_3 and C_3). The voltage-dependent capacitance (C_3) is plotted as $1/C^2$ in Fig. 3(c). A linear behavior is observed, and the slope gives an effective doping concentration of $N_D - N_A = 2 \times 10^{17}$ cm⁻³. Based on the expected N_D , N_A must be around 8×10^{17} cm⁻³, in good agreement with the reported value of 5×10^{17} cm⁻³ (Ref. 23). Evidently, the bias-dependent capacitance corresponds to the space charge layer at the junction. The remaining two RC elements are found to be bias-independent [red semicircles in Fig. 3(a)] and represent additional unknown barriers in the device structure, likely at the Ohmic contact and as a consequence of a native oxide interlayer. These additional barriers are responsible for masking the series resistance until 20 V.

Figure 4(a) shows the temperature-dependent forward bias I–V measurements. The I–V–T characteristics were evaluated using the thermionic emission model,

$$J=\,J_0\,\bigg[\,exp\,\bigg(\frac{qV}{\eta kT}\bigg)-1\bigg],$$

where η is the ideality factor and J_0 is the saturation current,

$$J_0 = A^{**} T^2 exp \bigg(-\frac{q \varphi_B}{kT} \bigg).$$

Here, T is the temperature, ϕ_B is the Schottky barrier height, k is the Boltzmann constant, and A^{**} is the reduced effective Richardson constant. The forward bias I–V as a function of temperature is shown in Fig. 4(a). The ideality factor and saturation current are found as a function of temperature by fitting the I–V characteristics to the thermionic emission model in the exponential region. An I–V barrier height of 1.9 eV is extracted from the slope of the Richardson plot, shown in Fig. 4(b). The value of 1.9 eV is in excellent agreement with the previous report of 2 eV by Reddy et al. ^{12,13} Additionally, the ideality factor is plotted against temperature in Fig. 4(c), which decreases from 1.5 at room temperature to 1.3 at 440 K. The exponential bias dependence of the current, the low ideality factor, and the extracted barrier height are all evidence for thermionic emission over the Schottky barrier and indicate that the I–V is dominated by the metal-semiconductor junction.

Interestingly, the current also increases with temperature in the series resistance region. To illustrate this, the current at $20\,\mathrm{V}$ forward bias is plotted vs $1/\mathrm{kT}$ in Fig. 4(d). The slope shows an activation energy of $\sim 300\,\mathrm{meV}$, which agrees with the activation energy of the Si donor obtained from temperature-dependent Hall measurements. This is strong evidence that, in the series resistance region (forward bias $> 20\,\mathrm{V}$), the current is limited by the resistivity of the Si-doped layer. It is interesting to note that a similar activation energy can be observed in the I–V characteristics of other reported AlN Schottky contacts. $^{6-9}$

Due to the refractory nature of AlN, it is expected that the Schottky contacts will be stable up to very high temperatures. Figure 5 shows the I–V characteristics of the device at room temperature before heating the sample, at 650 °C, at 700 °C, and at room temperature after heating the sample. With increasing temperature, the fraction of ionized Si donors increases exponentially; therefore, the current increases by several orders of magnitude. Evidently, the contacts are stable up to 650 °C, with close to four orders of magnitude rectification at this temperature. However, at

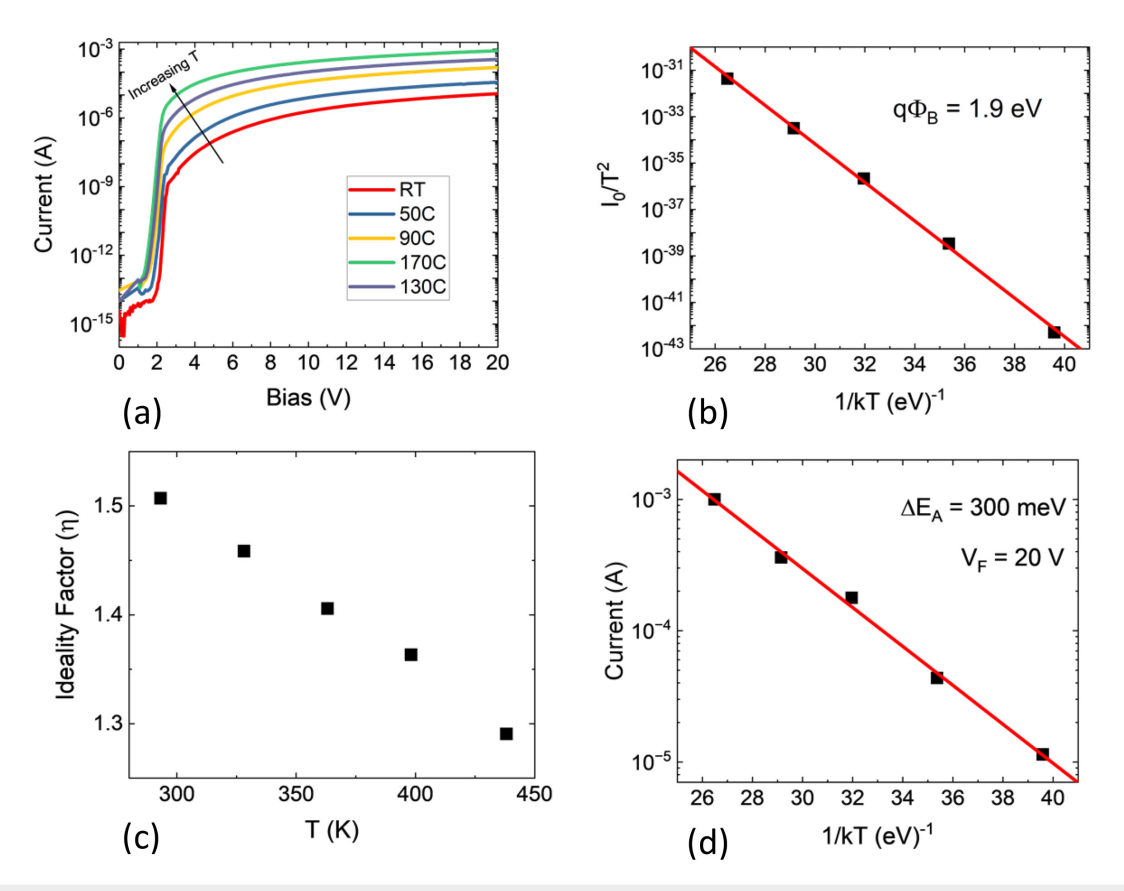


FIG. 4. (a) Temperature dependent forward bias I–V characteristics for the Si-doped AIN Schottky contact. (b) Richardson plot showing the extracted saturation current vs 1/kT and the extracted Schottky barrier height of 1.9 eV. (c) Ideality factor as a function of temperature. (d) Current at 20 V forward bias vs 1/kT. The slope gives an activation energy of around 300 meV

700 °C, there is a decrease in forward current, indicating degradation of the contact. After cooling down to room temperature, there is a change in the turn-on voltage, as seen in Fig. 5. However, there is still more than seven orders of magnitude rectification, and the

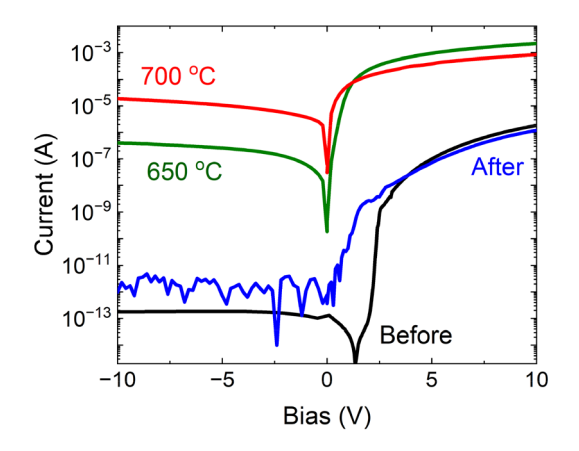


FIG. 5. I–V curve of Schottky diodes showing operation before, during and after 700 $^{\circ}\mathrm{C}$

forward bias I–V curves coincide after the turn on. These observations suggest that the voltage shift and degradation in performance after 700 °C is likely due to the alloying of the Ni/Au metal stack and not due to chemical degradation of the Si-doped AlN layer.

In summary, a low ideality factor of 1.5 was observed for Schottky contacts to AlN. A temperature-independent Schottky barrier height close to the expected value of around 2 eV is measured using temperature-dependent I-V. These results are strong evidence that current at low bias is due to the thermionic emission over the Schottky barrier. At higher bias, the current is limited mainly by the resistivity of the Si-doped layer. Using impedance spectroscopy, the space charge layer capacitance is isolated and the existence of two additional barriers is identified. Additionally, the contacts are observed to be stable up to 650 °C and maintain their rectifying behavior when cooled down to room temperature. Therefore, near-ideal diode behavior is observed in Schottky contacts to AlN, which is only possible due to the use of low-dislocation density native substrates in combination with controllably doped AlN layers. To illustrate the significance of these results, a benchmark plot is shown in Fig. 6, where the ideality factor is plotted as a function of room temperature barrier height for Schottky diodes on AlN. Although many challenges still remain, this Letter demonstrates the potential of AlN for power devices capable of operating in extreme environments.

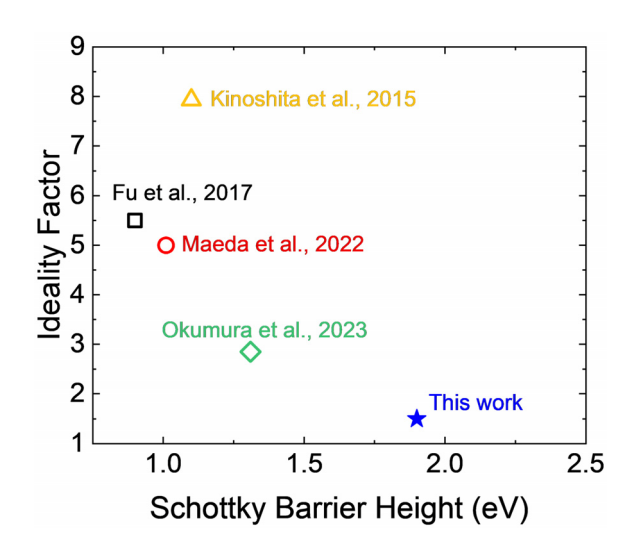


FIG. 6. Ideality factor vs barrier height for AIN Schottky diodes published in the literature. ^{6–10} Hollow and solid symbols represent temperature-dependent and independent Schottky barrier heights, respectively.

The authors gratefully acknowledge funding in part from ARO (No. W911NF-22-2-0171), AFOSR (Nos. FA9550-17-1-0225 and FA9550-19-1-0114), ARPA-E (No. DE-AR0001493), and NSF (Nos. ECCS-1508854, ECCS-1916800, and ECCS-1653383). C. E. Quiñones was supported by the NASA Space Technology Graduate Research Opportunity (No. NSTGRO 80NSSC22K1198).

AUTHOR DECLARATIONS Conflict of Interest

The authors have no conflicts to disclose.

Author Contributions

Cristyan E. Quiñones: Conceptualization (lead); Data curation (lead); (lead); (lead); Investigation analysis Methodology (lead); Writing - original draft (lead); Writing - review & editing (lead). Dolar Khachariya: Data curation (equal); Investigation (equal); Validation (equal); Writing - review & editing (equal). Pegah Bagheri: Data curation (equal); Formal analysis (equal); Investigation (supporting); Methodology (equal); Validation (equal); Writing - review & editing (equal). Pramod Reddy: Data curation (equal); Formal analysis (equal); Investigation (equal); Methodology (equal); Validation (equal); Writing – review & editing (equal). Seiji Mita: Data curation (equal); Formal analysis (equal); Investigation (supporting); Methodology (supporting); Validation (equal); Writing – review & editing (equal). Ronny Kirste: Conceptualization (supporting); Investigation (supporting); Methodology (supporting). Shashwat Rathkanthiwar: Writing – review & editing (supporting). James Tweedie: Funding acquisition (equal); Project administration (equal). Spyridon Pavlidis: Resources (equal); Writing - review & editing (equal). Erhard Friedrich Kohn: Data curation (equal); Formal analysis (equal); Investigation (equal); Methodology (equal); Validation (equal); Writing - review & editing (equal). Ramon Collazo: Funding acquisition (equal); Project administration (equal); Validation (equal); Writing - review & editing (equal).

Zlatko Sitar: Conceptualization (equal); Funding acquisition (equal); Project administration (equal); Resources (equal); Supervision (equal); Writing – review & editing (equal).

DATA AVAILABILITY

The data that support the findings of this study are available within the article.

REFERENCES

¹J. Y. Tsao, S. Chowdhury, M. A. Hollis, D. Jena, N. M. Johnson, K. A. Jones, R. J. Kaplar, S. Rajan, C. G. Van de Walle, E. Bellotti, C. L. Chua, R. Collazo, M. E. Coltrin, J. A. Cooper, K. R. Evans, S. Graham, T. A. Grotjohn, E. R. Heller, M. Higashiwaki, M. S. Islam, P. W. Juodawlkis, M. A. Khan, A. D. Koehler, J. H. Leach, U. K. Mishra, R. J. Nemanich, R. C. N. Pilawa-Podgurski, J. B. Shealy, Z. Sitar, M. J. Tadjer, A. F. Witulski, M. Wraback, and J. A. Simmons, "Ultrawide-bandgap semiconductors: Research opportunities and challenges," Adv. Electron. Mater. 4(1), 1600501 (2018).

²H. Amano, R. Collazo, C. D. Santi, S. Einfeldt, M. Funato, J. Glaab, S. Hagedorn, A. Hirano, H. Hirayama, R. Ishii, Y. Kashima, Y. Kawakami, R. Kirste, M. Kneissl, R. Martin, F. Mehnke, M. Meneghini, A. Ougazzaden, P. J. Parbrook, S. Rajan, P. Reddy, F. Römer, J. Ruschel, B. Sarkar, F. Scholz, L. J. Schowalter, P. Shields, Z. Sitar, L. Sulmoni, T. Wang, T. Wernicke, M. Weyers, B. Witzigmann, Y.-R. Wu, T. Wunderer, and Y. Zhang, "The 2020 UV emitter roadmap," J. Phys. D: Appl. Phys. 53(50), 503001 (2020).

³A. G. Baca, A. M. Armstrong, B. A. Klein, A. A. Allerman, E. A. Douglas, and R. J. Kaplar, "Al-rich AlGaN based transistors," J. Vac. Sci. Technol. A **38**(2), 020803 (2020).

⁴R. Rounds, B. Sarkar, D. Alden, Q. Guo, A. Klump, C. Hartmann, T. Nagashima, R. Kirste, A. Franke, M. Bickermann, Y. Kumagai, Z. Sitar, and R. Collazo, "The influence of point defects on the thermal conductivity of AlN crystals," J. Appl. Phys. 123(18), 185107 (2018).

⁵K. A. Jones, T. P. Chow, M. Wraback, M. Shatalov, Z. Sitar, F. Shahedipour, K. Udwary, and G. S. Tompa, "AlGaN devices and growth of device structures," J. Mater. Sci. 50(9), 3267–3307 (2015).

⁶Y. Irokawa, E. A. G. Víllora, and K. Shimamura, "Shottky barrier diodes on AlN free-standing substrates," Jpn. J. Appl. Phys. **51**(4R), 040206 (2012).

⁷T. Kinoshita, T. Nagashima, T. Obata, S. Takashima, R. Yamamoto, R. Togashi, Y. Kumagai, R. Schlesser, R. Collazo, A. Koukitu, and Z. Sitar, "Fabrication of vertical Schottky barrier diodes on n-type freestanding AlN substrates grown by hydride vapor phase epitaxy," Appl. Phys. Express 8(6), 061003 (2015).

⁸T. Maeda, R. Page, K. Nomoto, M. Toita, H. G. Xing, and D. Jena, "AlN quasivertical Schottky barrier diode on AlN bulk substrate using Al_{0.9}Ga_{0.1}N current spreading layer," Appl. Phys. Express 15(6), 061007 (2022).

⁹H. Fu, I. Baranowski, X. Huang, H. Chen, Z. Lu, J. Montes, X. Zhang, and Y. Zhao, "Demonstration of AlN Schottky barrier diodes with blocking voltage over 1 kV," IEEE Electron Device Lett. 38(9), 1286–1289 (2017).

¹⁰H. Okumura, Y. Watanabe, and T. Shibata, "Temperature dependence of electrical characteristics of Si-implanted AlN layers on sapphire substrates," Appl. Phys. Express 16(6), 064005 (2023).

¹¹P. Reddy, I. Bryan, Z. Bryan, J. Tweedie, R. Kirste, R. Collazo, and Z. Sitar, "Schottky contact formation on polar and non-polar AlN," J. Appl. Phys. 116(19), 194503 (2014).

¹²P. Reddy, I. Bryan, Z. Bryan, W. Guo, L. Hussey, R. Collazo, and Z. Sitar, "The effect of polarity and surface states on the Fermi level at III-nitride surfaces," J. Appl. Phys. 116(12), 123701 (2014).

¹³P. Reddy, I. Bryan, Z. Bryan, J. Tweedie, S. Washiyama, R. Kirste, S. Mita, R. Collazo, and Z. Sitar, "Charge neutrality levels, barrier heights, and band offsets at polar AlGaN," Appl. Phys. Lett. 107(9), 091603 (2015).

¹⁴R. Schlesser, V. Noveski, and Z. Sitar, US7678195B2 (16 March 2010).

¹⁵D. Ehrentraut and Z. Sitar, "Advances in bulk crystal growth of AlN and GaN," MRS Bull. 34(4), 259–265 (2009).

¹⁶R. Schlesser, R. Dalmau, and Z. Sitar, "Seeded growth of AlN bulk single crystals by sublimation," J. Cryst. Growth 241(4), 416–420 (2002).

- ¹⁷V. Noveski, R. Schlesser, B. Raghothamachar, M. Dudley, S. Mahajan, S. Beaudoin, and Z. Sitar, "Seeded growth of bulk AlN crystals and grain evolution in polycrystalline AlN boules," J. Cryst. Growth 279(1), 13–19 (2005).
- ¹⁸I. Bryan, Z. Bryan, S. Mita, A. Rice, J. Tweedie, R. Collazo, and Z. Sitar, "Surface kinetics in AlN growth: A universal model for the control of surface morphology in III-nitrides," J. Cryst. Growth 438, 81–89 (2016).
- ¹⁹ A. Rice, R. Collazo, J. Tweedie, R. Dalmau, S. Mita, J. Xie, and Z. Sitar, "Surface preparation and homoepitaxial deposition of AlN on (0001)-oriented AlN substrates by metalorganic chemical vapor deposition," J. Appl. Phys. 108(4), 043510 (2010).
- ²⁰P. Reddy, M. P. Hoffmann, F. Kaess, Z. Bryan, I. Bryan, M. Bobea, A. Klump, J. Tweedie, R. Kirste, S. Mita, M. Gerhold, R. Collazo, and Z. Sitar, "Point defect reduction in wide bandgap semiconductors by defect quasi Fermi level control," J. Appl. Phys. 120(18), 185704 (2016).
- ²¹P. Reddy, S. Washiyama, F. Kaess, R. Kirste, S. Mita, R. Collazo, and Z. Sitar, "Point defect reduction in MOCVD (Al)GaN by chemical potential control and a comprehensive model of C incorporation in GaN," J. Appl. Phys. 122(24), 245702 (2017).
- 22S. Washiyama, P. Reddy, B. Sarkar, M. H. Breckenridge, Q. Guo, P. Bagheri, A. Klump, R. Kirste, J. Tweedie, S. Mita, Z. Sitar, and R. Collazo, "The role of chemical potential in compensation control in Si:AlGaN," J. Appl. Phys. 127(10), 105702 (2020).

- ²³P. Bagheri, C. Quiñones-Garcia, D. Khachariya, S. Rathkanthiwar, P. Reddy, R. Kirste, S. Mita, J. Tweedie, R. Collazo, and Z. Sitar, "High electron mobility in AlN:Si by point and extended defect management," J. Appl. Phys. 132(18), 185703 (2022).
- ²⁴M. H. Breckenridge, P. Bagheri, Q. Guo, B. Sarkar, D. Khachariya, S. Pavlidis, J. Tweedie, R. Kirste, S. Mita, P. Reddy, R. Collazo, and Z. Sitar, "High n-type conductivity and carrier concentration in Si-implanted homoepitaxial AlN," Appl. Phys. Lett. 118(11), 112104 (2021).
- ²⁵H. Ahmad, Z. Engel, C. M. Matthews, S. Lee, and W. A. Doolittle, "Realization of homojunction PN AlN diodes," J. Appl. Phys. 131(17), 175701 (2022).
- ²⁶H. Ahmad, Z. Engel, C. M. Matthews, and W. A. Doolittle, "p-type AlN based heteroepitaxial diodes with Schottky, pin, and junction barrier Schottky character achieving significant breakdown performance," J. Appl. Phys. 130(19), 195702 (2021).
- ²⁷R. Dalmau, B. Moody, R. Schlesser, S. Mita, J. Xie, M. Feneberg, B. Neuschl, K. Thonke, R. Collazo, A. Rice, J. Tweedie, and Z. Sitar, "Growth and characterization of AlN and AlGaN epitaxial films on AlN single crystal substrates," J. Electrochem. Soc. 158(5), H530 (2011).
- 28P. Bagheri, P. Reddy, S. Mita, D. Szymanski, J. H. Kim, Y. Guan, D. Khachariya, A. Klump, S. Pavlidis, R. Kirste, R. Collazo, and Z. Sitar, "On the Ge shallow-to-deep level transition in Al-rich AlGaN," J. Appl. Phys. 130(5), 055702 (2021).